First-principles Study of Iron Oxyfluorides and Lithiation of FeOF

Vincent L. Chevrier,* Geoffroy Hautier,† Shyue Ping Ong, Robert E. Doe, and Gerbrand Ceder‡
Department of Materials Science and Engineering,
Massachusetts Institute of Technology, Cambridge, MA 02139, USA
(Dated: March 6, 2013)

First-principles studies of iron oxyfluorides in the FeF_2 rutile framework (FeO_xF_{2-x}, $0 \leq x \leq 1$) are performed using density functional theory (DFT) in the general gradient approximation (GGA) with a Hubbard U correction. Studies of O/F orderings reveal FeOF to be particularly stable compared to other FeO_xF_{2-x} ($x \neq 1$) structures, where FeF_2–FeOF mixing is not energetically favored. The band gap of FeF_2 is found to decrease as oxygen is substituted into its structure. The GGA+U electronic structure evolves from that of a Mott-Hubbard insulator ($x = 0$), to a charge transfer semiconductor ($x = 1$). Lithiation studies reveal that lithiation sites offering mixed O/F environments are the most stable. An insertion voltage plateau up to $Li_{0.5}FeOF$ on lithiation is found, in agreement with recent Li-ion battery experiments. The energetics of further lithiation with respect to conversion scenarios are discussed.

PACS numbers: 71.15.Mb,71.15.Nc,82.47.Aa

I. INTRODUCTION

Metal oxides and fluorides are used in myriads of applications such as electronics, energy storage and metallurgy, and in industrial processes such as the production of glasses, ceramics and lubricants.[1] The closeness in size and atomic number of the O^{2-} and F^- anions provides a bridge from fluorides to oxides and the properties of fluorides can often be altered or improved by oxygen-fluorine substitutions.

The possibility of altering the physical properties of a transition metal oxide or fluoride through oxygen-fluorine substitution motivates much of the interest in transition metal oxyfluorides. For example, in the field of Li-ion batteries, iron oxyfluorides have been recently characterized as high capacity positive electrode materials.[2] The FeO_xF_{2-x} positive electrode materials presented higher average voltages and better cycling than their unsubstituted FeF_2 counterparts.

This paper focuses on the impact of oxygen substitution into FeF_2 in the $0 < x \leq 1$ range for x in FeO_xF_{2-x}. FeF_2 possesses a tetragonal structure with space group symmetry $P4_2/mnm$ (136), this rutile-type structure is composed of a hexagonal close packed (hcp) anion lattice with cations occupying half of the octahedral sites. The unit cell of FeF_2 is shown in Fig. 1(a).

FeOF is traditionally synthesized through a solid state reaction of FeF_3 and Fe_2O_3 in an argon atmosphere at 950 °C.[3–6] The solid state synthesis of FeO_xF_{2-x} ($0 < x < 1$) solutions can be achieved by using FeF_2 and FeOF as precursors at 850 °C.[7] Solid solutions are achievable for $0 < x \leq 0.08$ and $0.71 \leq x \leq 1$, and a miscibility gap is observed for the $0.08 < x < 0.71$ range. X-ray diffraction experiments revealed that the FeO_xF_{2-x} structures maintain the FeF_2 rutile framework and the O and F atoms are distributed on the $4f$ sites, but were unable to establish any O/F ordering.[3,8]

Mössbauer studies later revealed the octahedral environment of the Fe atom in FeOF is consistently composed of 3 O^{2-} and 3 F^- anions, and the Fe atoms have an antiferromagnetic (AFM) ordering.[4,5] Electron diffraction experiments have shown evidence of an off-center shift of the Fe atoms suggesting an ordering of the O and F anions in the (110) and $(1\bar{1}0)$ planes with no correlation from one plane to the next.[6]

Recently, the synthesis of FeO_xF_{2-x} solid solutions ($0.3 \leq x \leq 1$) has been achieved through a low temperature solution process involving iron metal and a fluorosilic acid aqueous solution.[2] The FeO_xF_{2-x} powders obtained using this process have grain sizes on the order of 20 nm. Their structures were characterized through x-ray diffraction, confirming the FeF_2 rutile framework is maintained, but the O/F ordering was not investigated. The FeO_xF_{2-x} powders were used as positive electrode materials in a Li-ion electrochemical cell. *Ex-situ* x-ray diffraction studies of lithiated oxyfluorides suggested the presence of Li insertion into the FeO_xF_{2-x} grains without a significant change in lattice type for $Li_yFe_xO_{2-x}$, $0 < y \lesssim 0.5$. For $y > 0.5$ new peaks appeared in the x-ray diffraction patterns indicating the conversion to new crystal structures.

In this paper, the structural stability, anion distribution, and electronic structure of FeO_xF_{2-x} are studied using density functional theory with a Hubbard U correction (DFT+U). The most stable FeOF structure is then used for lithiation studies using DFT+U.

II. METHODS

A. Computational Methods

Density functional theory (DFT) calculations in the general gradient approximation with a Hubbard U correction (GGA+U) were performed. The rotationally invariant,[9] spherically averaged[10] formulation for the Hubbard correction was adopted.

Projector augmented wave (PAW)[11] pseudopoten-

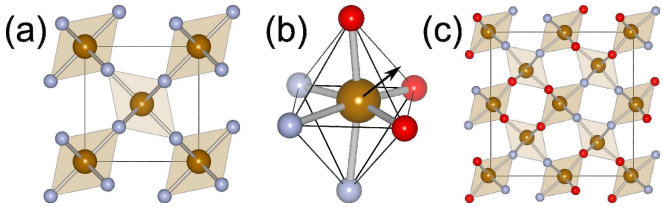

FIG. 1: (Color online) (a) Rutile FeF_2 ($P4_2/mnm$) in projection along [001]. (b) Fe octahedral environment in FeOF, the Fe moves off-center towards the O atoms.(c) Non-primitive cell of the lowest energy FeOF structure represented as a $2\times2\times1$ supercell of the FeF_2 structure with projection along [001]. See Table I for crystal structure details. Rendered using VESTA.[15]

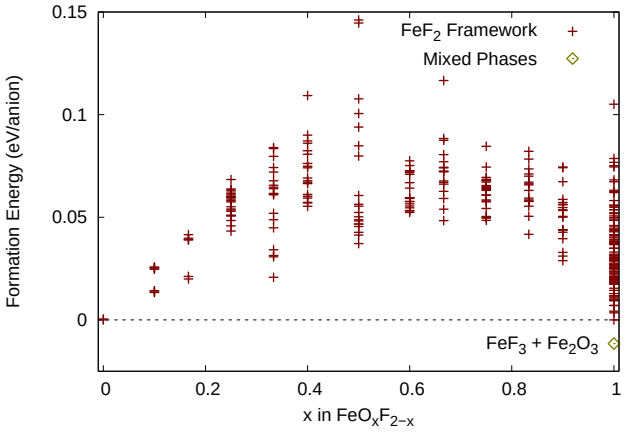

FIG. 2: (Color online) Formation energy as a function of oxygen content for FeO_xF_{2-x} structures in a FeF_2 rutile framework.

tials included in the Vienna Ab-initio Simulation Package (VASP 5.2.2) were used with the Perdew-Burke-Ernzerhof (PBE) functional.[12] In structures containing Fe and O or F, a value of $U = 4.0$ eV was used for Fe, which was obtained from fitting to experimental iron oxide formation energies.[13]

Spin-polarized total energy calculations and structure relaxations were performed with VASP using a 500 eV energy cut-off and appropriate k-point meshes to obtain a convergence of better than 10 meV per formula unit. Structural relaxations were performed to a tolerance of 2×10^{-4} eV/atom in the total energy. As in previous DFT studies of iron fluorides,[14] iron atoms were initialized in high spin ferromagnetic (FM) orderings for simplicity.

Results for the analysis of the electronic structure were obtained from static calculations using previously relaxed coordinates. The k-point density was doubled and no smearing was performed on band occupancies.

III. RESULTS

A. The FeO_xF_{2-x} Phase Diagram

The FeF_2 structure was taken as the basic lattice for the creation of new FeO_xF_{2-x} structures. Using an enumeration technique similar to the one proposed by Hart *et al.*,[16] structures were generated for $0 \le x \le 1$.

Ewald sums based on atomic charges O^{2-}, F^- and $Fe^{(x+2)+}$ were calculated for every generated structure.[17] At each discrete composition, the 20 structures yielding the lowest Ewald sums were chosen for further analysis using GGA+U.

In addition, a second set of structures with different O/F orderings were used for GGA+U calculations at the exact FeOF composition. Electron diffraction experiments on FeOF have shown evidence of a shift of the Fe atoms away from the octahedral center. This shift was suggested to be caused by the difference in Fe–O and Fe–F bond lengths and an ordering of the O and F anions in the (110) and $(1\bar{1}0)$ planes with no correlation from one plane to the next.[6] All the possible O/F orderings which satisfy this condition were attempted in supercells of up to $3\times3\times1$.

Figure 2 shows the formation energy of the FeO_xF_{2-x} structures in the FeF_2 rutile framework as a function of oxygen content. The formation energy is expressed in terms of eV/anion and is defined as

$$\frac{1}{2}E(\mathrm{FeO_xF_{2-x}}) - \frac{(1-x)}{4}E(\mathrm{FeF_2}) - \frac{x}{4}E_{\text{low-E}}(\mathrm{FeOF})$$

where E is the energy calculated using GGA+U and $0 \le x \le 1$. The range is limited to $0 \le x \le 1$ because structures with $x > 1$ have yet to be synthesized and the expression of the formation energy with FeOF as an end member facilitates the analysis. Figure 2 also shows the formation energies of FeF_3+Fe_2O_3, which, when averaged to the FeOF composition, has the lowest energy in the equilibrium phase diagram at $x = 1$. By definition, the number of Fe atoms present in structures following the FeO_xF_{2-x} formula allows for Fe^{2+}/Fe^{3+} charge ordering. Charge ordering, as evidenced by spin integration, was found in all calculated structures.

Figure 2 shows that when restricted to structures within the FeF_2 rutile framework, none of the iron oxyfluoride structures are lower in energy than a linear combination of FeF_2 and FeOF. The FeO_xF_{2-x} solid solution is therefore not favored for $0 < x < 1$ at least at low temperature, though entropic contributions may modify this at high temperature. The curvature displayed by the lower energy points in Fig. 2 also indicates that the energy penalty for a solid solution increases as one moves away from FeF_2 and FeOF.

The lowest energy structure obtained for FeOF is only 12 meV/anion above the corresponding combination of FeF_3 and α-Fe_2O_3. DFT yields 0 K formation energies, however the solid state synthesis of FeOF involves reacting FeF_3 and Fe_2O_3 at 950 °C.[6] The greater stability of the FeF_3–Fe_2O_3 two phase combination obtained computationally compared to the greater stability of FeOF at

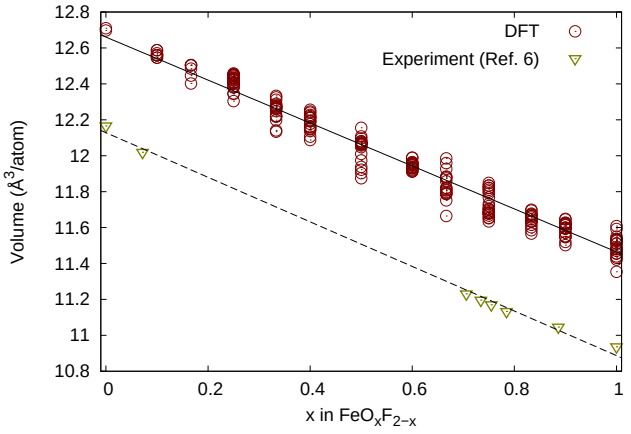

FIG. 3: (Color online) Variation in volume with increasing O substitution in FeF_2. The computational GGA+U results follow the same variation in volume as the experimental results of Ref. 7.

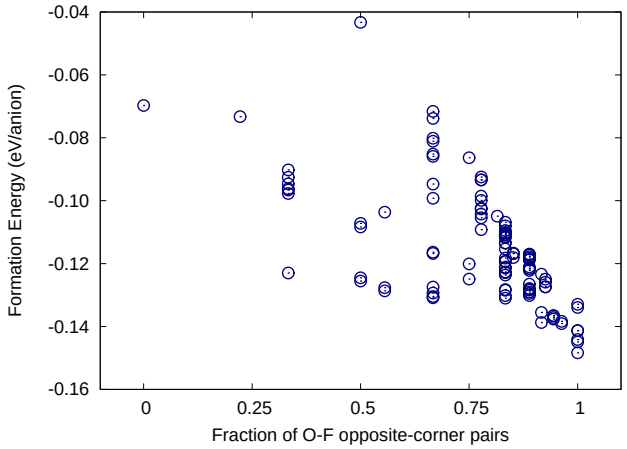

FIG. 4: (Color online) Formation energy as a function of O–F pairing across octahedral environments of Fe atoms in FeOF structures with various O/F orderings.

high temperature experimentally may be due to computational error but may also be due to entropic effects. According to Hautier *et al.*, 12 meV/anion would be within the standard deviation of these types of calculations.[18]

Both FeF_3 and Fe_2O_3 have well-ordered lattices typically free of vacancies and partial occupancies. On the other hand, FeOF has O and F atoms sharing the same lattice site. Above 0 K, the entropy contributions related to configurational disorder will be significantly greater for FeOF than for FeF_3 and Fe_2O_3.

An ideal solution model, where the O^{2-} and F^- species are two non-interacting species on a lattice, would yield an ideal entropy of mixing, $\Delta S^{\text{ideal}}_{\text{mixing}}$, given by

$$\Delta S^{\text{ideal}}_{\text{mixing}} = -k_B \left(\tfrac{1}{2}\ln\tfrac{1}{2} + \tfrac{1}{2}\ln\tfrac{1}{2}\right) \approx 0.060 \frac{\text{meV}}{\text{anion}\cdot\text{K}}, \quad (1)$$

where k_B is the Boltzmann constant. A temperature of 200 K would therefore be required to obtain 12 meV/anion. An ideal solution model leads to an overestimation of the entropy since, as is shown in the next section, the O^{2-} and F^- species do interact. Nevertheless, this order-of-magnitude estimate shows the difference in relative stability is on the scale of entropic contributions. Finally, other sources of entropy which are not discussed in this paper, such as vibrational entropy, may also play a role in the relative stability of FeOF.

Experimental investigations have found the volume of solid-state synthesized FeO_xF_{2-x} to be sensitive to O content, decreasing with increasing O content. The c axis contributes the most to the change in volume, evolving from $c(x = 0.0) = 3.308$ Å to $c(x = 1.0) = 3.044$ Å.[7] In a recent x-ray diffraction and electrochemical study of FeO_xF_{2-x}, the authors used the c parameter to determine the oxygen content of their structures.[2] Figure 3 shows the volume per atom with GGA+U for the FeO_xF_{2-x} structures compared to the experimental results. Good agreement is found in terms of the decrease in volume with increasing oxygen content, however the computational results are consistently greater than experiment by approximately 4%. This overestimation is very close to the median volume overestimation of 3% obtained when using GGA on a very large dataset.[19]

B. Oxygen-Fluorine Ordering in FeOF

The difference in length of the shorter Fe–O and the longer Fe–F bonds has been identified as the driving force for O and F orderings.[6] The O/F sites form an octahedron around the Fe atom. When O and F atoms are found in opposite corners of the octahedron, the Fe atom can relax towards the O atom. Figure 1(b) shows the O/F octahedron ordering which has all three F atoms at the vertices of one face of the octahedron and the O atoms at the vertices of the opposing face allowing the Fe atom to shift towards the O atoms. Figure 4 shows the energy in eV/anion of the FeOF structures as a function of the fraction of O–F opposite-corner pairs. The fraction of O–F opposite-corner pairs is obtained by considering each of the three pairs of opposite-corner atoms in the octahedron surrounding every Fe atom in the primitive cell, and counting those with an O on one side and an F on the other. Figure 4 shows that O–F opposite-corner pairs are one of the major factors affecting the stability of O/F orderings. The energy associated with O/F orderings is on the scale of 50 meV/anion.

The ordering proposed by Brink *et al.* for the (110) and $(1\bar{1}0)$ planes, with no correlation from one plane to the next, always yields structures where O atoms face F atoms in opposite corners of the octahedra. The FeOF structure yielding the lowest energy belongs to the class of structures respecting the ordering proposed by Brink *et al.* and is shown in Fig. 1(c). The ordering yields channels in the [001] direction which are composed solely of

TABLE I: Space group and Wyckoff positions of the lowest energy FeOF structure obtained.

$P4_2/m$ (84); $a = 6.6685$ Å, $c = 3.0689$ Å			
Atom	Site	x	y
Fe	$4j$	-0.22910	-0.23512
O	$4j$	-0.25667	0.05530
F	$4j$	0.25842	-0.44709

O atoms, of F atoms, or half O and half F. This arrangement allows the Fe atoms to relax towards the O atoms, with average Fe–O and Fe–F bond lengths of 1.93 Å and 2.12 Å respectively. At the same time, this O/F ordering allows the O channels to be 6% wider than the F channels. The lowest energy FeOF structure belongs to the $P4_2/m$ space group and its crystallographic information is listed in Table I.

C. Electronic Structure

Figure 5(a) shows the species-projected density of states (DOS) of FeF_2. The vast majority of the contributions to the Fe and F DOS are from d and p type orbitals, respectively. The Fe atoms in FeF_2 have a 2+ valence and a d^6 high-spin $t_{2g}^3(\uparrow)t_{2g}^1(\downarrow)e_g^2(\uparrow)$ electronic configuration. The $t_{2g}^1(\downarrow)$ states form the valence band and are clearly seen near the Fermi level. Since d states constitute the conduction and valence bands, FeF_2 is a Mott-Hubbard insulator.[20]

Figure 5(b) shows the DOS of a $3 \times 3 \times 3$ supercell of FeF_2 in which a single O atom was introduced ($Fe_{54}O_1F_{107}$). The anions in the FeO_xF_{2-x} rutile structure are three-fold coordinated by Fe cations. In this supercell, one of the three Fe–O bonds shortened to 1.79 Å while the other two remained near equilibrium length at 2.07 Å. The Fe belonging to the short Fe–O bond had a magnetic moment of 4.27 μ_B while the other two had the same magnetic moment (3.82 μ_B) as all the other Fe^{2+} atoms in the structure. The difference in magnetic moment indicates the Fe belonging to the shorter Fe–O bond is in a 3+ state while the other two remain in a 2+ state. The creation of an Fe^{3+} cation results in an empty $t_{2g}(\downarrow)$ state, which is seen in the gap of Fig. 5(b), leaving the Fe^{3+} in a high-spin $t_{2g}^3(\uparrow)e_g^2(\uparrow)$ state.

Figure 5(c) shows the DOS of the most stable FeOF structure obtained with GGA+U. The vast majority of the states occupied by Fe are spin up states, confirming the $t_{2g}^3(\uparrow)e_g^2(\uparrow)$ electronic configuration of Fe^{3+}. The valence band is predominantly populated by O electrons, and the F electrons are found at lower energies. The combination of a p valence band and d conduction band with a band gap of 1.5 eV makes FeOF a charge-transfer semiconductor.[20]

Figure 6 shows the band gap obtained for all structures as a function of x in FeO_xF_{2-x}, here x extends to 2 in order to highlight the decreasing trend of the band gap with increasing oxygen content. However, structures with $x > 1$ have not been experimentally observed. Band gaps obtained from the lowest energy structures are connected by a solid line, showing the lowest energy structures tend to have larger band gaps. Figure 6 also shows that structures with zero band gaps are obtained as early as $x = \frac{1}{6}$. GGA+U is known to generally underestimate band gaps, however, the evolution of the band gap with oxygen content should be representative of what is obtained experimentally.

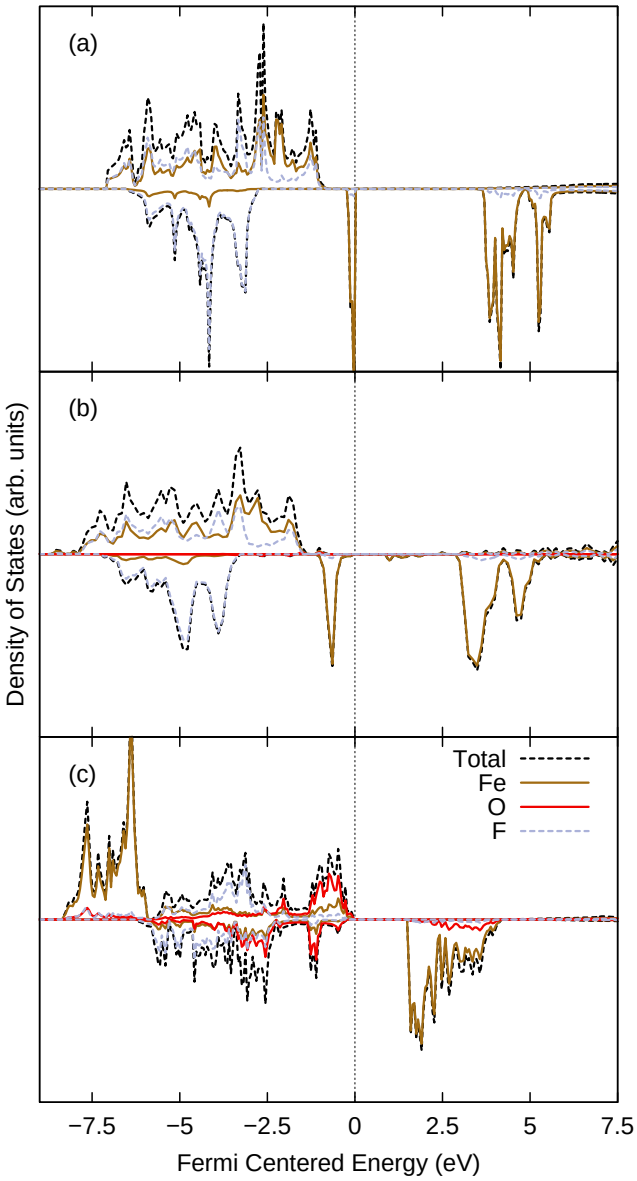

FIG. 5: (Color online) Density of states projected according to atomic species for (a) FeF_2, (b) $Fe_{54}O_1F_{107}$, and (c) FeOF.

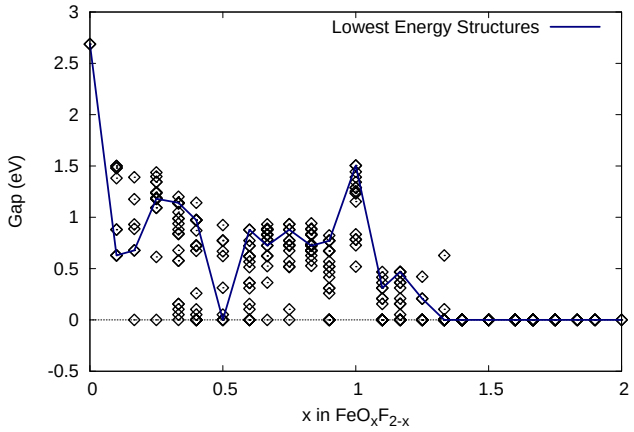

FIG. 6: (Color online) Evolution of the band gap as a function of x in FeO_xF_{2-x}. On average, the band gap decreases for $0 \leq x < 1$ and vanishes for $1.4 \leq x \leq 2$. Band gaps obtained from the lowest energy structures are connected by the solid line.

D. Lithiation of FeOF

The rutile structure provides suitable lithiation sites along the [001] channels formed by the anions and two off-channel tetrahedral sites described in more detail below. Previous theoretical and experimental studies of rutile $LiTiO_2$ have shown the sites found along the [001] channels to be significantly more energetically favorable.[21]

In the primitive cell of the $P4_2/mnm$ (136) rutile phase, the [001] channels offer lithiation sites found at Wyckoff positions $4c$ and $4d$, which respectively yield octahedral and tetrahedral anion environments. Along a given channel, neighboring tetrahedral and octahedral sites cannot be simultaneously occupied.

The lowest energy FeOF structure, detailed in Table I, was chosen for the study of Li insertion. In this structure with $P4_2/m$ (84) symmetry, the anion channels could hold Li atoms in the octahedral $2a$, $2b$, $2c$ and $2d$ sites or the tetrahedral $2e$, $2f$ and $4i$ ($z = \frac{1}{4}$) sites. Two other possible off-channel lithiation sites are the tetrahedral $4j$ sites with ($x \approx 0.26$, $y \approx 0.46$) or ($x \approx 0.25$, $y \approx 0.08$).

1. *Stability of lithiation sites*

In order to first assess the most likely initial lithiation site, the total energy was calculated for the addition of a single Li atom in a 2×2×2 supercell of FeOF in each of the possible sites, corresponding to a lithiation level of $Li_{1/32}FeOF$. Table II lists the lithiation sites from most to least stable. The two most stable lithiation sites are adjacent sites found in the mixed O/F channel, and differ by only 16 meV. Overall, the mixed O/F channel has the most stable sites, followed by the F channel, then the O channel and finally the off-channel tetrahedral sites.

TABLE II: Energetics of lithiation sites in a 2×2×2 supercell of FeOF.

			First Neighbors	
E (meV)	Site[a]	Site type	O	F
0	$2c$	oct	4	2
16	$4i$ (z=$\frac{1}{4}$)	tet	2	2
108	$2b$	oct	0	6
184	$2d$	oct	2	4
240	$2f$	tet	0	4
286	$2a$	oct	6	0
335	$2e$	tet	4	0
929	$4j$ (x=0.261, y=0.462)	tet	1	3
-[b]	$4j$ (x=0.25, y=0.08)	tet	3	1

[a]The primary cell Wyckoff site is used to identify the lithiation site, however only one Li atoms was present in the supercell.
[b]Li atom migrated to site $2c$

While one might expect the O channels to have been the most stable based on the electrostatic O^{2-}–Li^+ attraction, the Fe^{3+}–Li^+ repulsion appears to dominate the interaction. A symptom of this can be seen in the change in position of Fe atoms with lithiation. The nearest neighbor Fe atoms move away from the Li atoms by 0.18 Å on average, while the nearest neighbor anions remain near their original sites with an average change in distance from Li of only –0.06 Å.

The O channel is unfavorable because the Fe atoms, which have shifted off-center towards the O atoms, are too close to the Li atoms and the Fe^{3+}–Li^+ repulsion competes with the strong Fe–O bond. The O^{2-}–Li^+ attraction makes the site a local minimum but is insufficient to make it highly favorable.

The F channel has the advantage of having neighboring Fe atoms that are further out because they are off-center towards the O atoms. The Fe^{3+}–Li^+ repulsion needs only to compete with the weaker Fe–F bond, but the weaker F^-–Li^+ attraction only makes the site a local minimum.

The mixed O/F channel offers a balance of Fe^{3+} ions which are not too close and can shift away from the Li atoms without a large elongation of the Fe–O bonds, while mixed O^{2-}, F^- anions favor the electrostatic attraction with Li^+.

The off-channel tetrahedral sites can be eliminated as possible lithiation sites in agreement with previous studies of the TiO_2 rutile structure,[21] because they are either nearly 1 eV less favorable than the most favorable site or unstable.

In order to verify the electrostatic argument, purely electrostatic interactions were calculated through Ewald summations using the `pymatgen` (Python Materials Genomics) library.[17,22] Oxidation states of Li^+, Fe^{3+}, O^{2-}, and F^- were initially assigned. The electron donated by Li was assumed to be evenly distributed to the nearest neighbor Fe atoms in order to maintain charge neutrality. Ewald sums were performed on the final relaxed

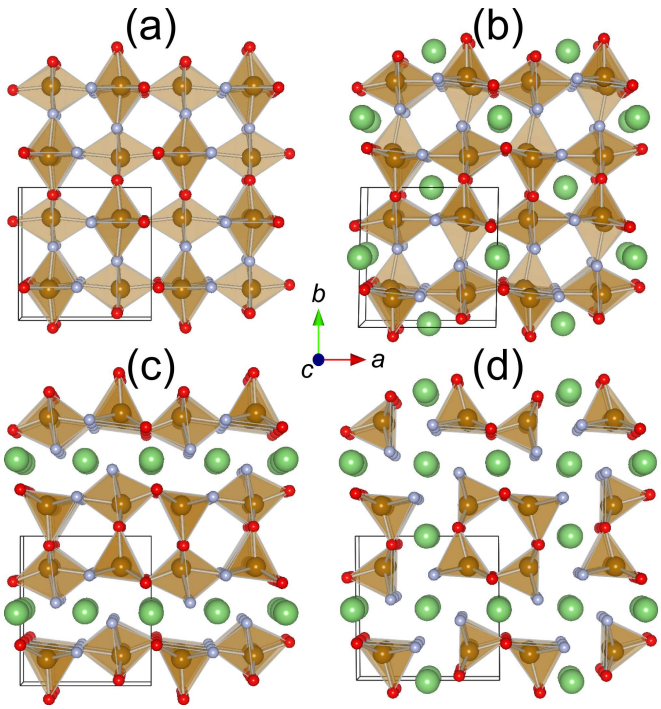

FIG. 7: (Color online) Lowest energy superstructures of (a) FeOF, (b) $Li_{0.25}FeOF$, (c) $Li_{0.5}FeOF$, (d) $Li_{0.75}FeOF$ in the [001] projection. Bond cutoff length set to 2.4 Å. See text for a description of lithiation sites.

structures obtained from DFT. The stability order of the lithiation sites obtained with electrostatics is the same as with DFT with the exception of the 2*d* site, which became the most stable. As a result, all the sites in the mixed O/F channels were most favored, followed by the F channels, the O channels, and finally the off-channel sites. Electrostatic interactions are therefore sufficient for predicting the stability order of lithiation sites when using DFT-relaxed structures.

2. *Lithiation orderings*

In order to study the lithiation of FeOF, Li orderings were attempted for y in Li_yFeOF (y = 0.25, 0.5, 0.75, 1). For a given Li ordering, all the lithiation sites were within anion channels and were either all tetrahedral or all octahedral. All the possible Li orderings respecting this criteria were attempted in the primitive cell and the 1×1×2 supercell for octahedral sites and only the primitive cell for tetrahedral sites.

Figure 7 shows the lowest energy orderings obtained for Li_yFeOF (y = 0.25, 0.5, 0.75). Figure 7(b) shows that lithiation occurs initially through the mixed O/F channels, in agreement with the stability of individual lithiation sites. In this 1×1×2 supercell the Li atoms are found in every other octahedral site along the O/F channels. Figure 7(c) shows that upon further lithiation to y = 0.5 the F channels become occupied. In this primitive cell, O/F and F channels are occupied causing significant expansion along the *b* axis. The lithiation sites are (0, $\frac{1}{2}$, 0) and ($\frac{1}{2}$, $\frac{1}{2}$, $\frac{1}{2}$). Bonds were drawn with a cutoff of 2.4 Å to highlight the separation between Fe and F atoms along the occupied channels. Figure 7 shows that for y = 0.75 all O/F and F channels are now fully occupied while the O channels remain vacant. In this primitive cell, Li occupies tetrahedral sites. The Fe atoms have now migrated even further from the F atoms and their coordination now resembles a square pyramid with a base containing two F and two O atoms. The lowest energy structure obtained for y = 1 is not shown, but contains one tetrahedral Li atom per primitive cell in every channel.

TABLE III: Evolution of average Fe–F and Fe–O bond lengths with lithiation in lowest energy structures for y in Li_yFeOF.

y	Fe–F (Å)	Fe–O (Å)	Δ_{Fe-F} (%)	Δ_{Fe-O} (%)
0	2.126	1.939	0.0	0.0
0.25	2.192	1.965	3.1	1.4
0.5	2.336	1.986	9.9	2.5
0.75	2.412	1.989	13.4	2.6
1	2.361	2.057	11.0	6.1

Table III shows the average nearest neighbor Fe–F and Fe–O bond lengths for the lowest energy lithiated structures. The average Fe–F bond length is seen to increase significantly more than the average Fe–O bond length, highlighting the migration of the Fe away from the F and towards the O as lithiation progresses. While the Fe–F average bond length is seen to decrease when going from y = 0.75 to y = 1, this structure is highly unstable compared to other stable phases as will be discussed later.

IV. DISCUSSION

A. FeO_xF_{2-x} and FeOF

Oxygen can be experimentally substituted into the FeF_2 rutile structure to create FeO_xF_{2-x} rutile oxyfluorides.[2–6]. As x increases, the structural and electronic properties of the oxyfluorides change.

Using DFT+U, the energies of over 500 FeO_xF_{2-x} structures were calculated in order to establish the relationship between phase stability and oxygen content. The results were in good agreement with experiment showing the FeOF structure is considerably more stable than compositions with different O/F ratios. While we find that a mix of FeF_3 and Fe_2O_3 has lower energy than FeOF, a simple solution entropy model shows that entropy contributions stemming from O and F configurational disorder could bridge the small gap in energy between FeOF and FeF_3+Fe_2O_3, possibly indicating the solid state synthesis of FeOF is entropy stabilized.

The stability of the FeOF structure compared to other O/F ratios stems from the octahedral geometry of the anion environment around the Fe cations and the difference in length between the shorter Fe–O bond and the longer Fe–F bond. Indeed, when oxygen and fluorine are present in equal quantities, the octahedral environment allows the O and F anions to be distributed in such a way as to let the Fe cation shift off-center to relax the Fe–O and Fe–F bonds. At the same time the rutile geometry permits every octahedron to be similarly occupied by O and F anions leading to Fe cations that are all in an equivalent 3+ state, and octahedra of constant size. Indeed, a mismatch in octahedral volumes can lead to a loss of stability. For example, the least stable structure of Fig. 4 found at $x = 0.5$ has two octahedra with mixed O/F sites, one octahedron with only O sites and another with only F sites. The mismatch in volumes between the larger FeF_6 octahedron and the smaller FeO_6 octahedron strains the bonding and leads to a loss of stability.

The GGA+U calculations confirm the findings of Brink *et al.*[6] regarding the O/F orderings. The suggested orderings of O and F atoms in the (110) and (1$\bar{1}$0) indeed yield the lowest energies. However, a wider exploration of the O/F orderings shows that orderings that are different from those suggested by Brink *et al.* can be within 20 meV/anion of the lowest energy orderings, roughly corresponding to the thermal energy available at room temperature (k_BT).

When using a low temperature synthesis route leading to a 20 nm grain size, Pereira *et al.* were able to obtain solid solutions from $x = 0.3$ to $x = 1$ in FeO_xF_{1-x},[2] unlike Brink *et al.* who observed a miscibility gap when employing a high temperature solid state synthesis route.[6] As one would normally expect higher temperatures to lead to more solid solution, it is possible that either Pereira's or Brink's samples are not fully equilibrated. An alternative explanation is that the relative penalty for creating a two-phase interface in the nanoparticles is too high, as for example has been shown to be the case in nano-sized $LiFePO_4$.[23]

Oxygen substitution into FeF_2 has a large effect on the electronic structure, indeed the material transitions from a Mott-Hubbard insulator to a charge-transfer semiconductor. In FeF_2, Fe d states form both the valence and conduction band. As oxygen is introduced in the structure Fe^{3+} atoms are created. The Fe d states forming the valence band are therefore emptied and initially appear as impurity states in the gap. One can therefore expect the insulating behavior of FeF_2 to be significantly reduced by O doping. When FeOF is reached, all the Fe d states that previously formed the valence band have been emptied and now form the conduction band. The O p states form the valence band, yielding a band gap on the order of 1.5 eV, approximately half the gap originally obtained with FeF_2, resulting in a charge transfer semiconductor .

As Fig. 5 indicates, the bandgap reduction is already significant for low amounts of oxygen, which is encouraging from the standpoint of prepaing more conductive oxygen-doped fluoride electrode materials.

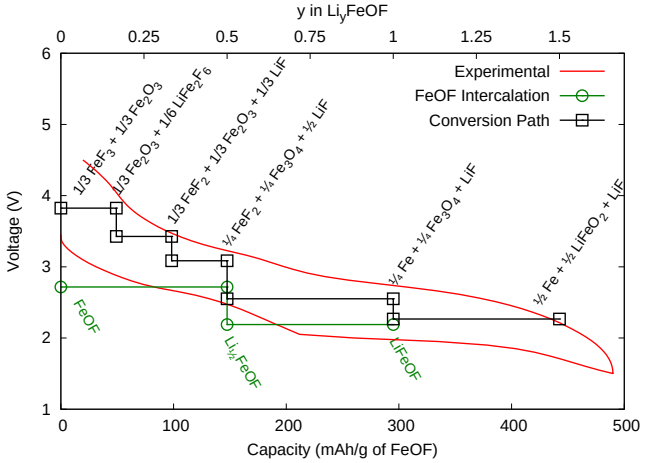

FIG. 8: (Color online) Comparison of voltage curves obtained from experiment,[2] from the DFT intercalation of Li into FeOF, and from the 0 K conversion path using the equilibrium phases in the Li-Fe-O-F phase diagram of the Materials Project.[24–26]

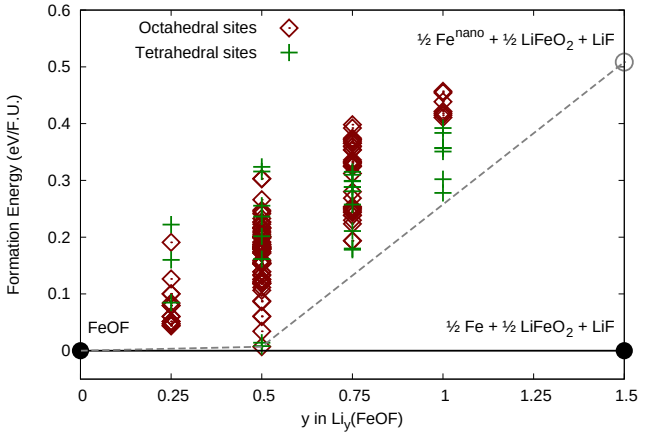

FIG. 9: (Color online) Formation energy of Li_yFeOF structures in terms of the FeOF and $\frac{1}{2}$Fe+$\frac{1}{2}$$LiFeO_2$+LiF end members. GGA and GGA+U calculations bridged using the methodology of Reference 27. Energy correction for nanoscale Fe adapted from Reference 14, see text for details.

B. Lithiation of FeOF

In a recent study of FeO_xF_{2-x} ($0 \leq x \leq 1$) as positive electrode materials for Li-ion batteries, Pereira *et al.* suggested that Li intercalation occurred in FeOF up to approximately $Li_{0.5}FeOF$ after which further lithiation leads to conversion. The study of the lowest energy O/F orderings in FeOF presented in this paper show the presence of O/F, O, and F channels along the [001] direction. These channels correspond to the usual diffusion path in

rutile-type structures.

Our lithiation studies demonstrate that anion channels are likely lithiated in the sequence: mixed channels, F channels, and finally O channels. The mixed O/F channels offer the most stable lithiation sites due to a combination of decreased Fe^{3+}–Li^{+} repulsion and significant anion–Li^{+} attraction.

A variety of Li orderings were attempted for multiple y in Li_yFeOF (y=0.25, 0.5, 0.75, 1) totaling 157 different orderings. The lowest energy ordering obtained at $y = \frac{1}{2}$ is significantly different from the ordering obtained in Ref. 21 for rutile $Li_{0.5}TiO_2$. Figure 7(c) shows the lowest energy ordering obtained for $Li_{0.5}FeOF$: one O/F channel and the F channel are filled with Li atoms occupying the (0, $\frac{1}{2}$, 0) and ($\frac{1}{2}$,$\frac{1}{2}$,$\frac{1}{2}$) positions respectively. On the other hand Koudriachova *et al.* found for $Li_{0.5}TiO_2$, a Li occupying an octahedral site in every channel, with all the Li atoms lined up on the same *ab* plane in every other primitive cell in *c*. This comparison indicates that the presence of F atoms significantly changes the lithiation behavior as well as the behavior of the host metal cation.

Insight into the lithiation of FeOF can be obtained by contrasting the intercalation of Li into the FeOF structure, which has been discussed up to this point, with the conversion path. The conversion path corresponds to the linear combination of equilibrium phases of the Li-Fe-O-F phase diagram yielding the desired Li_yFeOF composition. The conversion path for a given chemical system can be easily obtained from the Materials Project,[24] indeed the Phase Diagram App allows the creation of grand potential phase diagrams that are open to one element. The equilibrium voltage curve for a conversion reaction involving Li can therefore be obtained by making the phase diagram open to Li and tracking the equilibrium phases of a given composition as a function of Li chemical potential.[25,26] This approach is known to yield results in excellent agreement with experiment for Si and Sn-based Li-ion[28,29] or Na-ion[30] alloy anodes. The Li-Fe-O-F phase diagram can therefore allow us to obtain a voltage profile stemming from the conversion path. However, the Materials Project uses $U = 5.3$ for Fe as opposed to the $U = 4$ used here.[19] In order to allow direct comparison of results, all phases in the Li-Fe-O-F phase diagram were obtained using the Materials Project REST API[22] and their total energies recalculated using the methodology described above in "Computational Methods".

Figure 8 shows the conversion voltage path (in black) obtained from the Li-Fe-O-F phase diagram plotted along with the experimental voltage curve (the conversion voltage obtained directly from the Materials Project is essentially identical but lower by approximately 0.25 V). The voltage for intercalation is also shown in green. According to the Li-Fe-O-F phase diagram calculations, the 0 K equilibrium phases at the end of lithiation are $\frac{1}{2}$Fe+$\frac{1}{2}$$LiFeO_2$+LiF. Here $LiFeO_2$ refers to the γ-$LiFeO_2$ polymorph with space group $I4_1/amd$ (141). Note that the experimental data was obtained from an 85 wt % iron oxyfluoride, 15 wt % activated carbon nanocomposite.[2] The capacity in Fig. 8 was calculated assuming the activated carbon was inactive and may therefore be slightly overestimated.

In order to illustrate the energetics of the Li orderings in intercalated FeOF, the energies of the Li_yFeOF structures are plotted in Fig. 9 in terms of the FeOF and $\frac{1}{2}$Fe+$\frac{1}{2}$$LiFeO_2$+LiF end members, which define the equilibrium tie line in the phase diagram along this composition axis, and approximately correspond to the phases that are experimentally observed before and after lithiation, as discussed below. Previous studies have shown that the equilibrium phases can typically only be used as guides for conversion reactions involving oxides and fluorides because of size and kinetic effects.[14,31] In their study of the conversion reactions of iron fluorides with Li, Doe *et al.* were able to improve their agreement with experiment by taking into account the 1.0168 eV per Fe atom cohesive energy penalty resulting from 1 nm sized Fe particles. Recent scanning transmission electron microscope (STEM) studies of lithiated iron oxyfluorides have confirmed the presence of nanoscale Fe regions at full lithiation.[32] Figure 9 therefore also shows the formation energy of the end member when taking into account the energy penalty for nano-sized Fe.

Both Fig. 8 and Fig. 9 indicate that the stable phases at all levels of lithiation are "conversion phases" though the energy difference with Li-intercalated FeOF phases is small. Given that the kinetic barriers to conversion reactions (nucleation) are much larger than for intercalation (diffusion) it seems reasonable to assume that the system does intercalate lithium to a certain extent before it converts, which is indeed what is seen in experiments.[2] From the comparison between the calculated and experimentally measured potentials in Fig 8, and the relative energy plot in Fig. 9, one may be able to get an indication of how FeOF lithiates and converts.

The calculated intercalation potential from FeOF to $Li_{0.5}FeOF$ agrees remarkably well with experiments. In addition, Fig. 9 shows that the driving force for conversion in this concentration range is small, making intercalation very likely. From $Li_{0.5}FeOF$ to LiFeOF the intercalation potential is again in reasonable agreement with the experimentally measured voltage, even though conversion is detected in experiments as $y > 0.5$ in Li_yFeOF. Combining the experimental and computed information may lead us to a hypothesis for the lithiation mechanism of Li_yFeOF for $y > 0.5$: Note from Fig. 9 that $\frac{1}{2}Fe^{nano}$+$\frac{1}{2}$$LiFeO_2$+LiF only becomes an equilibrium phase for $y > 0.5$, note also from Fig. 9 that there are no stable intercalated states between $y = 0.5$ and $y = 1$, as the energy of the state with $y = 0.75$ is above the tie line that connects the $y = 0.5$ and $y = 1$ states. This indicates that metastable intercalation of Li_yFeOF for $y > 0.5$ would likely proceed as a two-phase reaction, forming LiFeOF as soon as $y > 0.5$, neglecting the small amount of Li excess that may exist in $Li_{0.5}FeOF$. However, our calculations indicate that this LiFeOF is sufficiently unstable with respect to decomposition into

Fe, LiF and $LiFeO_2$ to allow for the creation of nano-sized Fe. We will comment on these decomposition products later as they are not exactly what is seen experimentally.

Hence, our hypothesis for the reaction mechanism of FeOF with lithiation is as follows: FeOF takes up lithium through intercalation in a homogeneous solid solution-type reaction up to about $Li_{0.5}FeOF$. At that point, further Li uptake is through a two-phase intercalation reaction to LiFeOF, with the LiFeOF product rapidly decomposing to LiF, Fe and a third Li-Fe-O phase. Note that at least the first part of this statement is in agreement with experiments where stable intercalation is seen up to $Li_{0.5}FeOF$. In our proposed mechanism, intercalated LiFeOF forms through a two-phase reaction from $Li_{0.5}FeOF$, and then rapidly decomposes, hence no intercalation past $y > 0.5$ would be observed. Because metastable LiFeOF and its decomposition products would form immediately for $y > 0.5$ (due to the two-phase nature of the intercalation reaction), conversion products would be seen as soon as $y > 0.5$.

Conversion of metastable LiFeOF should be fairly easy. Because the material has a Li/F ratio of 1, LiF can form on a very small scale as no long-range diffusion is required. This transformation can therefore occur faster than if transforming between phases with different compositions. Indeed Fig. 7 and Table III show that the local structure evolution with Li intercalation is consistent with the eventual formation of LiF and $LiFeO_2$. The Fe atoms are seen abandoning the F atoms in favor of the O atoms as the Li content increases.

This reaction hypothesis leaves unanswered what the precise nature of the conversion products of LiFeOF is. Pereira *et al.*[2] observed LiF, Fe, and a rocksalt-like phase of approximate composition $Li_{1.7}Fe_2O_3$ with main diffraction peaks at 37, 43, and 62.3° in 2θ. Our suggestion of the γ-$LiFeO_2$ polymorph is based on the stable phases present in the Materials Project and is likely to miss defect phases that form as part of the conversion process. However, the distinction between Pereira's phase and γ-$LiFeO_2$ may not be that large. The main x-ray diffraction peaks of γ-$LiFeO_2$ are 37.97, 41.23, 44.67, 62.40°. Also, its cation-disordered polymorph α-$LiFeO_2$ ($Fm3m$),[33] has main peaks at 37.45, 43.59, 63.29°, which is in good agreement with the observed values given the broadness of the experimental peaks, and gives further support for the presence of a rocksalt type structure.

The DFT energies, the experimental capacity, and the experimental diffraction peaks lend support to the presence of $LiFeO_2$ at the end of lithiation. Recently, extensive experimental studies were performed on lithiated $FeO_{0.7}F_{1.3}$.[32] Electron energy loss spectroscopy (EELS) and STEM measurements allowed the authors to establish the presence of $Fe+Li_xFe^{n+}O_yF_z+LiF$ at 1.5 V, where $n = 2.3$. Assuming a phase ratio identical to the one predicted with the Materials Project, the phases obtained would be $\frac{1}{2}Fe+\frac{1}{2}LiFe^{n+}O_{1.4}F_{0.6}+LiF$, which with typical oxidation states would yield $n = 2.4$ in excellent agreement with experiment. Our predictions are therefore consistent with the most recent experimental results. Further experimental studies will be necessary to confirm the presence of $LiFeO_2$ at 1.5 V when lithiating stoichiometric FeOF.

Finally, the effect of O substitution on Li diffusion barriers in the anion channels has not been studied in this paper, though it is likely to be substantial. Recent studies of Li diffusion in Tavorite structures showed that the valence of both the anion and the metal cation had a large impact on the diffusion barriers.[34] Careful study of diffusion barriers in FeOF and in oxyfluorides in general may provide guidance for the design of conversion materials.

V. CONCLUSION

First-principles studies of iron oxyfluorides in the FeF_2 rutile framework (FeO_xF_{2-x}, $0 \leq x \leq 1$) were performed. Studies of O/F orderings reveal FeOF to be particularly stable compared to other FeO_xF_{2-x} ($x \neq 1$) structures. The high temperature required for the experimental solid state synthesis of FeOF and the energy difference with respect to decomposition products (FeF_3, Fe_2O_3) suggests that FeOF may be entropy stabilized. GGA+U calculations are also used to study the electronic structure as a function of oxygen content, revealing a shrinking of the band gap as oxygen is substituted into FeF_2. The GGA+U electronic structure evolves from that of a Mott-Hubbard insulator ($x = 0$), to a charge transfer semiconductor ($x = 1$).

Lithiation studies reveal that lithiation sites offering mixed O/F environments are the most stable. We speculate that homogeneous intercalation occurs up to $Li_{0.5}FeOF$ followed by formation of LiFeOF through a two-phase reaction from $Li_{0.5}FeOF$ with LiFeOF rapidly decomposing into LiF, Fe, and another Li-Fe-O phase.

VI. ACKNOWLEDGMENTS

This work was supported as part of the Northeastern Center for Chemical Energy Storage (NECCES), an Energy Frontier Research Center funded by the US Department of Energy, Office of Science, Office of Basic Energy Sciences under Award Number DE-SC0001294. The authors would like to thank the members of the NECCES for valuable discussions and access to experimental data, especially Nathalie Pereira and Prof. Glenn Amatucci.

* current address: 3M Electronics Markets Materials, 3M Center, St Paul, MN 55144, USA

† current address: Institut de la Matière Condensée et des

Nanosciences (IMCN)-Nanoscopic Physics (NAPS), Université Catholique de Louvain, Belgique
‡ Electronic address: gceder@mit.edu
[1] P. Hagenmuller, ed., *Inorganic Solid Fluorides*, Materials Science and Technology (Academic Press, 1985).
[2] N. Pereira, F. Badway, M. Wartelsky, S. Gunn, and G. G. Amatucci, J. Electrochem. Soc. **156**, A407 (2009).
[3] P. Hagenmuller, J. Portier, J. Cadiou, and R. DePape, C. R. Acad. Sci. **260**, 4768 (1965).
[4] J. Chappert and J. Portier, Solid State Commun. **4**, 185 (1966).
[5] J. Chappert and J. Portier, Solid State Commun. **4**, 395 (1966).
[6] F. J. Brink, R. Withers, and J. Thompson, J. Solid State Chem. **155**, 359 (2000).
[7] F. J. Brink, R. Withers, and L. Norén, J. Solid State Chem. **161**, 31 (2001).
[8] M. Vlasse, J. C. Massies, and G. Demazeau, J. Solid State Chem. **8**, 109 (1973).
[9] A. I. Liechtenstein, V. I. Anisimov, and J. Zaanen, Phys. Rev. B **52**, R5467 (1995).
[10] S. L. Dudarev, G. A. Botton, S. Y. Savrasov, C. J. Humphreys, and A. P. Sutton, Phys. Rev. B **57**, 1505 (1998).
[11] P. E. Blöchl, Phys. Rev. B **50**, 17953 (1994).
[12] J. P. Perdew, K. Burke, and M. Ernzerhof, Phys. Rev. Lett. **77**, 3865 (1996).
[13] L. Wang, T. Maxisch, and G. Ceder, Phys. Rev. B **73**, 195107 (2006).
[14] R. E. Doe, K. A. Persson, Y. S. Meng, and G. Ceder, Chem. Mater. **20**, 5274 (2008).
[15] K. Momma and F. Izumi, J. Appl. Crystallogr. **44**, 1272 (2011).
[16] G. L. W. Hart and R. W. Forcade, Phys. Rev. B **77**, 224115 (2008).
[17] P. P. Ewald, Annalen der Physik **64**, 253 (1921).
[18] G. Hautier, S. P. Ong, A. Jain, C. J. Moore, and G. Ceder, Phys. Rev. B **85**, 155208 (2012).
[19] Materials Project Wiki, accessed November 23, 2012, URL https://materialsproject.org/wiki/index.php.
[20] J. Zaanen, G. A. Sawatzky, and J. W. Allen, Phys. Rev. Lett. **55**, 418 (1985).
[21] M. V. Koudriachova, N. M. Harrison, and S. W. deLeeuw, Phys. Rev. B **65**, 235423 (2002).
[22] S. P. Ong, W. D. Richard, V. L. Chevrier, G. Ceder, A. Jain, M. Kocher, S. Cholia, K. A. Persson, and G. Hautier, Comput. Mater. Sci. (2012), accepted.
[23] M. Wagemaker, F. M. Mulder, and A. van der Ven, Adv. Mater. **21**, 2703 (2009).
[24] Phase Diagram App (v0.3), Materials Project (DB 2012.11.19), accessed November 23, 2012, URL http://www.materialsproject.org.
[25] S. P. Ong, L. Wang, B. Kang, and G. Ceder, Chem. Mater. **20**, 1798 (2008).
[26] S. P. Ong, A. Jain, G. Hautier, B. Kang, and G. Ceder, Electrochem. Commun. **12**, 427 (2010).
[27] A. Jain, G. Hautier, S. P. Ong, C. J. Moore, C. C. Fischer, K. A. Persson, and G. Ceder, Phys. Rev. B **84**, 045115 (2011).
[28] I. A. Courtney, J. S. Tse, O. Mao, J. Hafner, and J. R. Dahn, Phys. Rev. B **58**, 15583 (1998).
[29] V. L. Chevrier and J. R. Dahn, J. Electrochem. Soc. **156**, A454 (2009).
[30] V. L. Chevrier and G. Ceder, J. Electrochem. Soc. **158**, A1011 (2011).
[31] R. E. Doe, K. A. Persson, G. Hautier, and G. Ceder, Electrochem. Solid-State Lett. **12**, A125 (2009).
[32] F. Cosandey, D. Su, M. Sina, N. Pereira, and G. G. Amatucci, Micron **43**, 22 (2012).
[33] A. E. Abdel-Ghany, A. Mauger, H. Groult, K. Zaghib, and C. M. Julien, J. Power Sources **197**, 285 (2012).
[34] T. Mueller, G. Hautier, A. Jain, and G. Ceder, Chem. Mater. **23**, 3854 (2011).